Int. J. Heat Mass Transfer. Vol. 28, No. 9, pp. 1669–1678, 1985
Printed in Great Britain

0017–9310/85 $3.00 + 0.00

Heat and mass transfer in wood during drying

O. A. PLUMB,* G. A. SPOLEK† and B. A. OLMSTEAD*

* Department of Mechanical Engineering, Washington State University, Pullman, WA 99164, U.S.A.
† Department of Mechanical Engineering, Portland State University, Portland, OR 97207, U.S.A.

(*Received* 23 *March* 1984 *and in final form* 12 *February* 1985)

Abstract—A model for heat and mass transport in softwood is developed. The model includes liquid transport via capillary action as well as diffusion. The model is unique in that transport properties which in some cases are both not available in the literature and difficult to measure are developed from knowledge of wood structure. Calculated results compared favorably with those determined experimentally. The experimental results represent the first of their kind in that moisture profiles are measured during the drying process using gamma attenuation.

INTRODUCTION

DIMENSIONAL lumber must be dried from its green condition to achieve structural stability. This drying is commonly done by blowing hot air or steam over lumber stacked in a kiln. Experience has shown that serious cracking, warping, and fiber collapse occur if the wood is dried too fast. However, if the drying operation lasts too long, excessive energy and time costs decrease productivity of the plant. In order to quantify the factors that control lumber drying, researchers have developed analytic and empirical models to describe movement of water through wood during drying. Sherwood [1] assumed that moisture movement through a solid porous media such as wood is due to gradients of the moisture content, and used Fick's second law of diffusion to predict the unsteady concentration of water. Good agreement with experimental data followed when the diffusion coefficient could be written as an appropriate function of moisture content and the range of moisture contents predicted was less than the fiber saturation point (FSP), which corresponds to the moisture content below which all water molecules are chemically bound to the cellulose.

At moisture contents greater than the FSP, the additional water must exist as liquid water and as water vapor in the voids or lumens in the wood cells. These cells are long and narrow, hollow in the center, and overlap one another on ends that taper shut. On the overlapping surfaces, there are small orifices or pits that provide fluid paths between adjacent cell lumens. This morphology suggests that the capillary mechanisms that allow motion of nutrient fluids in the living tree may also control movement of the free liquid in wood during drying [2]. Luikov [3] developed a set of coupled partial differential equations to describe the heat and mass transport in capillary porous media by assuming that the transfer of moisture is analogous to heat transfer and that capillary transport is proportional to gradients in moisture and temperature. The resulting transport coefficients are strong functions of both temperature and moisture content, as well as wood species and drying conditions. Thus, extensive experimental programs are required to determine the coefficients necessary to analyze a wide variety of woods and drying methods.

Two major impediments to development of predictive models for transport in wood exist. First, detailed experimental data quantifying both drying rates and moisture and temperature distributions within wood during drying have not been available. This deficiency has been overcome to a small extent by the experimental program which has accompanied the model development efforts to be discussed in this paper. Second, the necessary transport properties have received little attention.

In the present study, a set of governing equations that describe both capillary and diffusive transport of moisture during wood drying, as well as the transfer of heat, are developed and solved numerically. By developing these equations from first principles, the transport coefficients that arise are dependent on documented transport properties and wood structure. Represenstative values for these properties were taken from the literature and used to predict drying and heating rates for a typical piece of lumber, as well as the moisture and temperature profiles across the board section. These values are compared to data taken under actual drying conditions to demonstrate the efficiency of the predictive model.

THEORETICAL MODEL

Wood in its green state can be considered a three-phase mixture: solid cell wall material (with bound water to the FSP), free liquid that partially fills the lumens, and gas bubbles containing air and water vapor that occupy the remaining lumen space. Each phase represents a continuum, and its behavior can be predicted through use of the conservation laws, however, a different set of governing point equations will arise for each phase and there is no way of knowing

NOMENCLATURE

C	transport coefficient
c_p	specific heat
D	effective diffusion coefficient
EMC	equilibrium moisture content
FSP	fiber saturation point
g	gravitational constant
h_{lg}	latent heat of vaporization
K	permeability
k	effective thermal conductivity
L	board half-thickness
M	moisture content
$\dot{m}$	mass transfer rate
p	pressure
$\dot{q}$	heat transfer rate
r	radius of curvature
S	saturation
T	temperature
t	time
v	velocity
X	dimensionless moisture content
z	spatial variable.

Greek symbols

β	mass transfer correction factor
γ	specific gravity
θ	dimensionless temperature
μ	dynamic viscosity
ρ	density
σ	surface tension
ϕ	void fraction
ψ	phase volume fraction.

Subscripts

a	air
c	capillary
conv	convective
g	gas phase
h	heat transfer
l	liquid phase
m	mass transfer
max	maximum
0	initial condition
wv	water vapor
∞	ambient condition.

a priori in which phase an arbitrary point lies and, therefore, which set of equations is appropriate. In order to achieve a single set of governing equations that is valid throughout the wood, the phase equations need to be volume averaged to include the effect of each phase on the whole. Whitaker [4] has developed the methods for performing this volume averaging for drying processes and his results will be utilized here for wood.

In order to employ this approach to develop the governing equations of drying, certain approximations and assumptions must be made. It is assumed that, due to the length of the lumber compared to its thickness, a one-dimensional model for heat and moisture transport can be employed. Hence, we are interested in transport in the radial direction (normal to the growth rings) or the tangential direction (tangential to the growth rings) and not the longitudinal direction, which would be the vertical for a standing tree (see Fig. 1). The cell wall material is assumed to be rigid above the FSP [5] with constant density. Both liquid and gas phase motion are slow, so convective accelerations can be ignored. Within the averaging volume, the thermal conductivity is assumed to be constant, as is the specific heat, so enthalpy is a linear function of temperature. In addition, it is assumed that both reversible work and viscous dissipation are negligible, and that there is no internal heat source, although such a factor to account for electromagnetic heating can readily be included.

Behavior of moisture in the drying wood is described by the continuity equations for the liquid phase and the water vapor portion of the gas phase. Since it is the total water content that is of interest, these equations can be added together to yield an equation for the total free moisture content, neglecting surface diffusion of bound water, in the form

$$\phi\frac{\partial S}{\partial t}+\frac{\partial}{\partial z}\left(v_l+\frac{\rho_{wv}}{\rho_l}v_g\right)=\frac{\partial}{\partial z}\left(\frac{\rho_g}{\rho_l}D\frac{\partial}{\partial z}\frac{\rho_{wv}}{\rho_g}\right). \quad (1)$$

Here, S is the dimensionless liquid saturation or the fraction of the void space filled with water, and is defined by

$$S=(\psi_l\rho_l+\psi_g\rho_{wv})/\phi\rho_l. \quad (2)$$

Development of the volume-averaged thermal energy equation for each phase, and their subsequent summation yields the total thermal energy equation [6]

$$\rho c_p\frac{\partial T}{\partial t}+(\rho_l c_{pl}v_l+\rho_g c_{pg}v_g)\frac{\partial T}{\partial z}+\dot{m}h_{lg}=\frac{\partial}{\partial z}\left(k\frac{\partial T}{\partial z}\right), \quad (3)$$

where ρ is the spatial average density

$$\rho=\psi_s\rho_s+\psi_l\rho_l+\psi_g(\rho_{wv}+\rho_a) \quad (4)$$

and c_p is the mass fraction average specific heat

$$c_p=[\psi_s\rho_s c_p+\psi_l\rho_l c_{pl}+\psi_g(\rho_{wv}c_{pwv}+\rho_a c_p)]/\rho. \quad (5)$$

Arrival at this total energy equation requires the simplifying assumption of local thermal equilibrium—locally the temperature of each phase is the same. The criteria for the validity of this assumption [7] are easily satisfied by the slow process of wood drying.

Equations (1) and (3) constitute the set of governing differential equations used to describe heat and mass transfer during wood drying. Each equation includes

both diffusive and convective components. In order to solve these equations, the convective liquid- and gas-phase velocities must be determined by solving the phase momentum equations. On dimensional grounds [8], this solution must be a form of Darcy's law, the volume average of which can be shown [9] to depend on the phase pressure gradient and permeability, K, as

$$v_g = -\frac{K_g}{\mu_g}\left(\frac{\partial p_g}{\partial z} - \rho_g g\right) \tag{6}$$

$$v_l = -\frac{K_l}{\mu_l}\left(\frac{\partial p_l}{\partial z} - \rho_l g\right). \tag{7}$$

Darcy's law is known to be a good approximation for single-phase flow through wood [10], and it is assumed valid for two-phase flow based on experience with unsaturated flow through other media [11].

Use of Darcy's law to eliminate the convective velocities introduces as unknowns the respective phase pressures and permeabilities. The permeability of many woods to both gas and liquid flow has been measured, although there is some uncertainty surrounding the permeability in unsaturated flow. Pressures in the liquid and gas phases are more difficult to identify. It is reasonable to quantify gas-phase pressure by assuming that the air in the phase behaves as an ideal gas while the water vapor is assumed to be in saturated equilibrium with the free water, using the Kelvin equation to correct for effects of surface curvature on vapor pressure. In this manner, the gas-phase pressure gradient can be written as being proportional to gradients in the saturation and the temperature [6]. The liquid-phase pressure, however, is more elusive. It is convenient to use the concept of capillary pressure p_c to relate the gas- and liquid-phase pressures by

$$p_c = p_g - p_l. \tag{8}$$

Capillary pressure, in turn, can be expressed in terms of the mechanistic model, to be discussed later, so the liquid pressure can be totally eliminated.

Following arguments presented elsewhere [6], it is now possible to write the moisture continuity and thermal energy equations entirely in terms of two dependent variables S and T:

$$\phi\frac{\partial S}{\partial t} - \frac{\partial}{\partial z}\left\{\left[\frac{K_l}{\mu_l}(C'_s - C_s) + \frac{\rho_{wv}}{\rho_l}\frac{K_g}{\mu_g}C'_s + \frac{\rho_g}{\rho_l}DC''_s\right]\right.$$
$$\times\frac{\partial S}{\partial z} + \left[\frac{K_l}{\mu_l}(C'_T - C_T) + \frac{\rho_{wv}}{\rho_l}\frac{K_g}{\mu_g}C'_T + \frac{\rho_g}{\rho_l}DC''_T\right]$$
$$\left.\times\frac{\partial T}{\partial z} - \left(\frac{K_l}{\mu_l}\rho_l + \frac{K_l}{\mu_g}\rho_g\right)g\right\} = 0 \tag{9}$$

$$\rho C_P\frac{\partial T}{\partial t} - \left\{\frac{\rho c_{pl}K_l}{\mu_l}\left[(C'_s - C_s)\frac{\partial S}{\partial z} + (C'_T - C_T)\frac{\partial T}{\partial z} - \rho_l g\right]\right.$$
$$\left. + \frac{\rho_g c_{pg}K_g}{\mu_g}\left[C'_s\frac{\partial S}{\partial z} + C'_T\frac{\partial T}{\partial z} - \rho_g g\right]\right\}$$
$$\times\frac{\partial T}{\partial z} + \dot{m}h_{lg} = \frac{\partial}{\partial z}\left(k\frac{\partial T}{\partial z}\right) \tag{10}$$

where

$$C_s = \frac{\partial p_c}{\partial S} \tag{11}$$

$$C_T = \frac{\partial p_c}{\partial T} \tag{12}$$

$$C'_s = \frac{\partial p_g}{\partial S} \tag{13}$$

$$C'_T = \frac{\partial p_g}{\partial T} \tag{14}$$

$$C''_s = \frac{\partial(\rho_{wv}/\rho_g)}{\partial S} \tag{15}$$

$$C''_T = \frac{\partial(\rho_{wv}/\rho_g)}{\partial T}. \tag{16}$$

MECHANISTIC MODEL

In contrast to the random packing of many porous media, such as sand, wood cells are organized in a very regular pattern. This fact makes it very attractive to utilize a mechanistic model of wood structure to identify capillary porous properties—permeability and capillary pressure. Permeability, or fluid conductivity, depends on the distribution of pits and the number of cell walls that must be traversed. The capillary pressure depends on the shape of the gas–liquid menisci within the cellular voids, hence on the size and shape of the cells. In light of these considerations, the mechanistic model was constructured to reflect the observed morphology of wood and the measured permeability behavior.

Structure of a typical softwood is shown in Fig. 1. In the longitudinal (L) direction, which would be vertical for a standing tree, the cells have a cross-section which is approximately square. These cells are tapered shut at the ends on the tangential faces where they overlap adjacent cells. Most of the interconnecting pits are on these overlapping faces. Interspersed throughout this regular pattern of longitudinal cells are clusters of ray cells—equally long, but of smaller diameter than

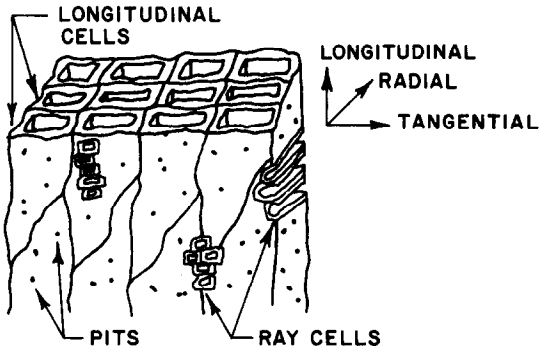

FIG. 1. Structure of a typical softwood.

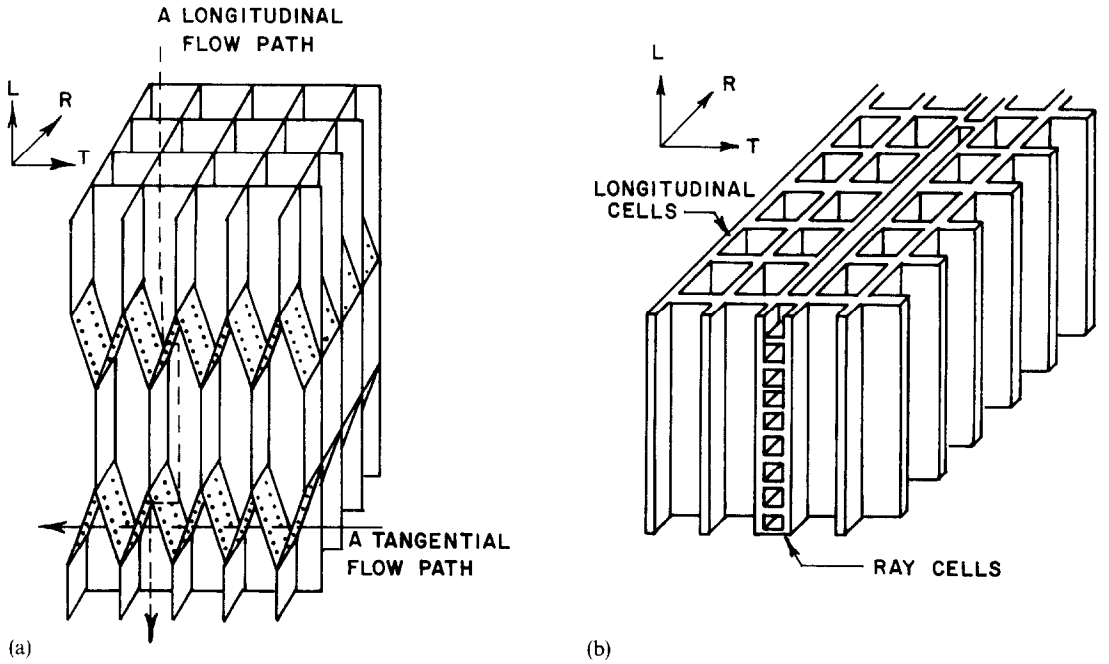

FIG. 2. Mechanistic models of softwood structure: (a) tangential transport and (b) radial transport.

longitudinal cells and radially oriented. The ray cells are also interconnected among themselves and with the longitudinal cells through pits.

The mechanistic models of softwood structure are also illustrated in Fig. 2. As can be seen, different geometries are assumed to capture the salient features of directional transport. The tangential model is based on the model developed by Comstock [12] to predict the measured ratio of directional permeabilities to single-phase flow. For this model, all pits are located on the tapered overlapping portions of square longitudinal cells. Ray cells are not included since they do not contribute to transport in the tangential direction. The radial model also incorporates square longitudinal cells tapered at the end (not shown), but includes arrays of smaller, square, ray cells. The pits connecting ray cells to each other and to adjacent longitudinal cells are assumed to be uniformly distributed.

Green wood, prior to drying, contains sufficient moisture to partially fill the cellular void space, and it is commonly assumed that this free liquid recedes to the ends of the cells to surround a central gas bubble [13]. Figure 3 illustrates probable distribution of the liquid. As can be seen, the principle radii of curvature of a given meniscus depends on the amount of liquid contained and size of the cell. Since density of the water vapor in the gas phase is much less than that of the liquid, it is reasonable to assume that

$$S = \frac{\psi_1}{\phi} \tag{17}$$

so that the saturation is a measure of the local liquid content.

The capillary pressure depends on the curvature according to

$$p_c = \sigma\left(\frac{1}{r_1} + \frac{1}{r_2}\right) \tag{18}$$

where σ is surface tension, and r_1 and r_2 are the principle radii of curvature. Since r_1 and r_2 depend on saturation and σ depends on temperature, $p_c = f(S, T)$. The functional form of this dependency has been developed elsewhere [6, 14] and has been verified in isothermal experiments [15]. Hence, the capillary pressure can be expressed in terms of the cell geometry of a given softwood.

Permeability of wood to single-phase flow has been measured extensively [10, 12, 16–18], yielding well-documented values for the saturated permeability in

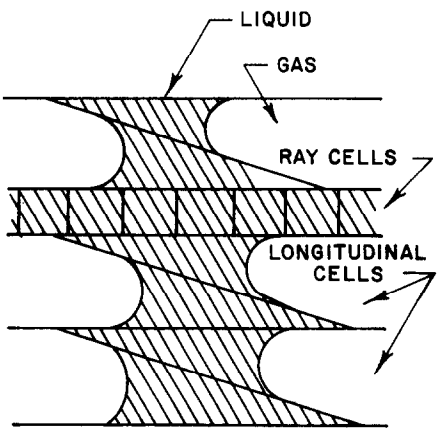

FIG. 3. Assumed moisture location in lumens.

each direction. The unsaturated permeability $K(S)$ of the mechanistic model can be related to the saturated permeability, which defines the total number of pits available for flow, and to the saturation, which determines the fraction of the pits that are covered with liquid and capable of transmitting liquid. Because of the tapered surfaces, $K(S)$ is a weakly nonlinear function [6], but a linear dependency is assumed here for simplicity. The same mechanistic structure was utilized to develop the dependence on saturation and temperature of the effective thermal conductivity $k(S, T)$.

The gas-phase permeability, since it depends on the distribution and size of pits, should be the same as liquid-phase permeability; this has been confirmed experimentally for single-phase flow [12]. However, during drying the recession of the menisci causes about 95% of the pits to become aspirated or occluded [18] so the gas-phase permeability will be 5% or less (depending on saturation) of the single-phase permeability. As a result, the liquid-phase velocity and gas-phase velocity will be of the same order of magnitude for similar pressure gradients. Since the density of the gas phase is much smaller than the liquid, convection of both energy and mass due to gas motion can be neglected as a first approximation.

Initial numerical work described in [6] presented solutions to equations (9) and (10) except that gravitational transport was neglected on the basis of a comparison of the order of magnitude of the gravitational term to that for liquid convection driven by capillary action. Data is available for the effective diffusion coefficient for moisture in wood below the fiber saturation point as a function of moisture content and temperature [23, 24]. Since bound water and water vapor cannot be separated experimentally, the experimentally measured diffusion coefficients include both. Hence, the transport coefficients C_s'' and C_T'' are incorporated into a single effective diffusion coefficient. Since a typical lumber-drying process is relatively slow, one might expect that vapor-phase pressure-driven transport might be negligible. The results presented in [6] indicate that some pressure build-up does occur initially due to temperature gradients, but does not have a significant impact on the end result. The conclusion drawn is that C_s' and C_T' can be neglected in a practical lumber-drying model. Dependence of surface tension of water on temperature is relatively weak. This, coupled with the fact that temperature gradients are significant only during a short period during the onset of drying, leads to elimination of the term involving C_T. Finally, it is assumed that all evaporation occurs at the surface, thus, the latent heat term in equation (10) appears only in the boundary condition. During the early phase of the drying process, capillary transport of liquid to the surface dominates. It is important that the drying process be sufficiently slow to preclude the existence of a drying front which would result in the pit asperation phenomena discussed earlier, inhibiting drying in the later stages. After the surface reaches the fiber saturation point, moisture must diffuse to the surface through the lumens and cell walls, with evaporation of bound water finally occurring at the surface. These arguments are presented elsewhere [6, 14, 19].

Defining dimensionless dependent variables as

$$\theta = \frac{T-T_0}{T_\infty - T_0} = \frac{T-T_0}{\Delta T}$$

(dimensionless temperature) (19)

$$M = S(M_{max} - \text{FSP}) + \text{FSP} = S\Delta M + \text{FSP}$$

(dimensionless moisture content) (20)

results in the moisture content, M, including both free water and bound water. Incorporating these variables and the assumptions given above results in a relatively simple model which includes only diffusion and capillary transport

$$\frac{\phi}{\Delta M}\frac{\partial M}{\partial t} + \frac{\partial}{\partial z}\left(\frac{K_l}{\mu_l} C_s \frac{\partial M}{\partial z}\right) = \frac{\partial}{\partial z}\left(\frac{\partial M}{\partial z}\right) \quad (21)$$

$$\rho C_p \frac{\partial \theta}{\partial t} + \rho_l c_p \frac{K_l}{\mu_l}\frac{C_s}{\Delta M}\frac{\partial M}{\partial z}\frac{\partial \theta}{\partial z} = \frac{\partial}{\partial z}\left(k\frac{\partial \theta}{\partial z}\right). \quad (22)$$

It can be noted that the continuity equation is decoupled from the energy equation, except for the temperature dependence of the transport coefficients, implying negligible thermally-driven mass transport. By contrast, the energy equation is coupled to continuity through the liquid-phase convection of thermal energy.

Boundary conditions necessary for solution of the governing equations are formulated by assuming that convective heat and mass transfer occur at the board surface and that there is no heat or mass flux through the midplane at a distance L from the surface. Hence,

$$@\ z = L, \quad \frac{\partial M}{\partial z} = 0 \quad (23)$$

$$\frac{\partial \theta}{\partial z} = 0 \quad (24)$$

$$\frac{d}{dt}\int_0^L M(z)\, dz = -\dot{m}_{conv} \quad (25)$$

$$\frac{d}{dt}\int_0^L \rho C_p \theta(z)\, dz = \dot{q}_{conv} - h_{lg}\dot{m}_{conv}. \quad (26)$$

Integral formulation of the surface flux boundary condition was chosen over differential formulation to enhance stability of the numerical solution.

The surface convection of heat $\dot{q}_{conv}$ can be expressed as

$$\dot{q}_{conv} = h_h \Delta T(1-\theta) \quad (27)$$

where h_h is the overall heat transfer coefficient. Its value can be determined from empirical correlations for turbulent channel flow which are typical of kiln operation. The surface convection of mass can also be written as

$$\dot{m}_{conv} = h_m(p_{wv}|_{z=0} - p_{wv_\infty}) \quad (28)$$

where h_m is the overall mass transfer coefficient, $p_{wv}|_{z=0}$ is the partial pressure of water vapor at the surface and p_{wv_∞} is the ambient condition. The value of h_m can be determined from h_h by analogy if the surface is saturated as an open liquid surface would be. The wood surface is not fully saturated [20, 21] and the mass flux at the surface, hence the drying rate, depends on the surface moisture content as well. Neither theoretical models nor experimental results with general applicability are currently available for mass transfer coefficients for unsaturated porous hygroscopic surfaces.

To circumvent this problem a series of experiments involving southern pine were conducted, in which drying rates and moisture contents as near to the surface as possible were measured using gamma attenuation. An empirical correction factor to the convective mass transfer coefficient, $\beta(X)$, defined as

$$\dot{m}_{conv} = \beta(X) h_m (p_{wv}|_{z=0} - p_{wv_\infty}) \tag{29}$$

where

$$X = \frac{M|_{z=0} - \text{EMC}}{M_{max} - \text{EMC}} \tag{30}$$

was extracted from the experimental results. The resulting form of $\beta(X)$ which was used in the numerical calculations is shown in Fig. 4. The use of this result naturally forces considerable feedback between theory and experiment. However, the exact functional form of $\beta(X)$ is not critical to lumber drying, since the moisture transport is internally controlled.

NUMERICAL SOLUTION

The nonlinearities of the governing equations (21) and (22) necessitated use of a digital computer to generate an approximate solution. A finite difference, implicit numerical scheme was employed. At each time increment, the nodal values of M and θ were solved iteratively and convergence was checked on both variables. Underrelaxation was employed at each iteration to quicken the convergence.

Initially, the temperature and moisture content were set to be equal at all nodes at the value corresponding to measured wood conditions. Boundary condition values were based on experimental conditions. Typical time increments were 1800 s, while typical spatial increments were 0.05 cm.

EXPERIMENTAL STUDY

Experiments were conducted in a laboratory scale simulation of actual kiln conditions. The experimental setup consisted of a heated wind tunnel supplying hot air to a floating test section containing a single 2 × 4 (3.8 × 8.9 cm) 45-cm long. A cross-section of the test section is shown in Fig. 5. The test section is supported by a load cell, thus allowing weight loss to be measured as a function of time.

Local temperatures within the wood were measured using thermocouples implanted in holes drilled prior to the test. Local moisture contents were measured using gamma attenuation. A 570 mCi ^{241}Am-source was placed behind a brass plate containing a collimating slit 0.51-mm high and 2.79-cm wide. A NaI (T1) scintillating crystal integrally mounted to a photomultiplier tube was placed on the opposite side of the test section. This gamma detector assembly was shielded from background radiation, except for a 0.51-mm-high by 3.81-cm-wide collimator slit which was aligned with the slit on the source side. The entire source/detector assembly was mounted on a common frame which would be traversed in the vertical direction using a stepping motor (0.44 mm/step).

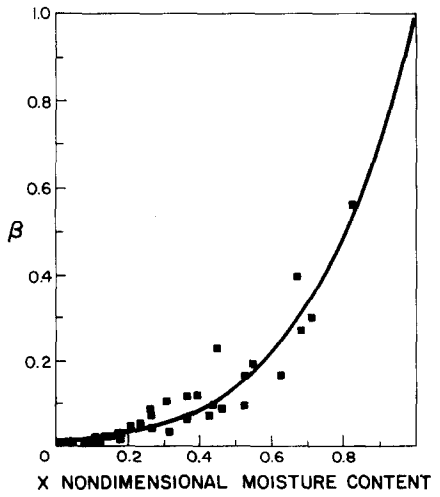

FIG. 4. Convective mass transfer correction factor as a function of moisture content.

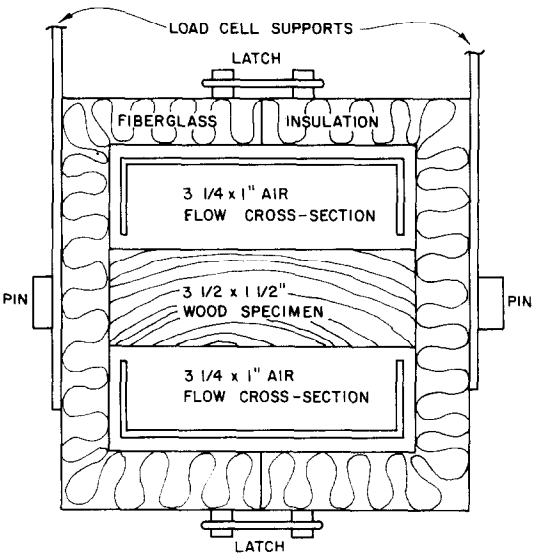

FIG. 5. Cross-section of experimental test section.

The uncertainty in measurement of moisture content using this approach is moisture dependent. Using worst-case assumptions, it was estimated [21] that uncertainties ranged from $\pm 6.8\%$ at $\pm 120\%$ moisture content to 29.5% at 10% moisture content.

Since a single drying experiment could run for several days, the entire data acquisition process was computerized. The experimental setup, uncertainty analysis, and results for southern pine are discussed in detail by Brown [21] and Plumb *et al.* [22].

RESULTS AND DISCUSSION

The numerical program was run under conditions corresponding as closely as possible to experimental conditions. It was difficult to select a representative value for the permeability because the drying direction was never totally parallel nor perpendicular to the drying surface, due to growth ring curvature in the test samples. Hence, moisture movement was never purely radial nor tangential, but rather some combination of the two; radial permeability is as much as two orders of magnitude greater than the tangential permeability of southern pine. The program was run using different permeability values to demonstrate its effect on drying. Values of the other transport coefficients used in the calculations are summarized in Table 1, along with a reference to the appropriate source.

Figure 6 shows a comparison of the prediction of the drying model with experimental results for moisture content as a function of time. The inset illustrates the specimen's grain orientation, which deviates significantly from the purely radial direction. The contribution of tangential transport implies that the lower permeability (10^{-12}) should more accurately predict the overall drying rate, as appears to be the case. The greater permeability representative of the radial direction predicts faster drying than was measured.

Temperature histories at the surface and the center of the board shown in Fig. 6 indicate that the model overpredicts the temperature for both values of permeability. This is attributed to heat losses from the test section, as opposed to inadequacies in the model.

Figure 7 shows comparable curves for a wood specimen dried at a lower air temperature, thus slower drying. Grain orientation for this specimen allows more uniform radial transport of heat and mass, and the corresponding higher permeability gives the model better agreement with the data. Temperatures are again overestimated with both permeability inputs; fluctuations in the temperature data arise from diurnal variations in temperature in the laboratory.

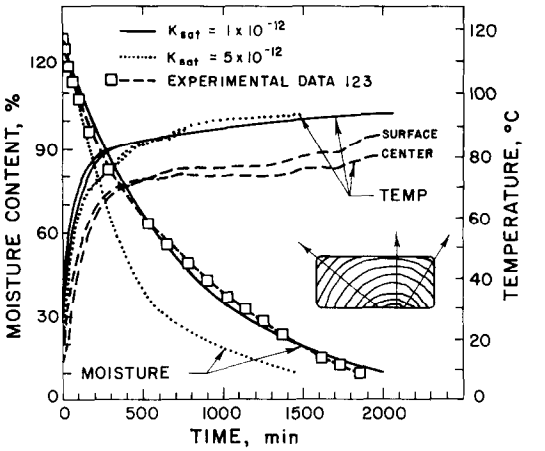

FIG. 6. Comparison of experimental and predicted results for wood sample No. 123.

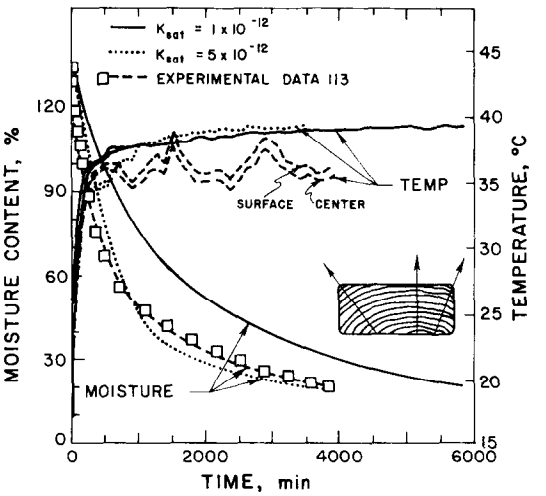

FIG. 7. Comparison of experimental and predicted results for wood sample No. 113.

Table 1. Transport properties utilized in numerical calculations

Property	Model	Source
D, diffusion coefficient, $cm^2\ s^{-1}$	$D = \exp(3.746 - 5.12\gamma - 4317/T)$ (K)	[24]
C_s, capillary transport coefficient, $g\ s^{-2}\ cm^{-1}$	$C_s = \begin{cases} = 0 & S > 0.802 \\ = \dfrac{\sigma}{2.7 \times 10^{-3}} \left(\dfrac{0.802}{S}\right)^{3/2} & S < 0.802 \end{cases}$	[6, 15]
σ, surface tension, $g\ s^{-2}$	$\sigma = 75.64 - 0.144T$ gm s^{-2}	[27]
k, thermal conductivity, cal $cm^{-1}\ s^{-1}\ K^{-1}$	from thermal network model supported by experimental results	[6, 14, 25, 26]

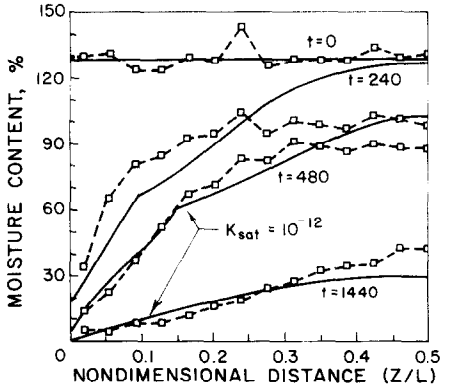

FIG. 8. Comparison of experimental and predicted moisture profiles for wood sample No. 123.

The ability of the numerical model to predict moisture distribution in the wood is of great interest because, due to water-induced swelling of wood, moisture gradients cause strain gradients that can lead to cracking and warping. Moisture profiles predicted for various times during the drying cycle are shown, with moisture contents measured at corresponding times, in Figs. 8 and 9. The measured moisture profiles exhibit surprising oscillations. These are explainable to a certain extent if the corresponding density measurements are examined. Peaks in moisture content occur coincident with valleys in density and vice versa. The less dense earlywood has a larger lumen volume than the dense latewood. Thus, at the same saturation level, the earlywood will have a higher moisture content than latewood. One can speculate that, if the moisture distributions shown in Figs. 8 and 9 could be converted to saturation, the curves would be smooth; hence, indicative of saturation-gradient-driven liquid transport due to capillary action. Since wood is both highly nonhomogeneous and non-isotropic, it is likely that the transport is not strictly one-dimensional. Thus, a one-dimensional model that assumes homogeneity in a single direction cannot be expected to capture the detailed features of the drying process. It is hoped that such a model can provide quantiative results on a more global basis that are of utility.

For both specimens shown, the model tends to overpredict moisture content at the center of the board early in the drying. This result may be a consequence of the assumption that the gas-phase permeability is sufficient to dissipate gas-pressure gradients. If early local heating causes the gas pressure to rise significantly above the ambient pressure, then additional liquid flow will be driven by gas-phase pressure and moisture contents will decline more quickly. This argument is supported by the fact that the board heats up faster than it dries, as indicated by Figs. 6 and 7.

As previously mentioned, saturated liquid permeability has a large effect on drying time. This parameter is a factor, of course, only at moisture contents greater than the fiber saturation point when mobile free liquid exists. To quantify this effect, the model was used to predict drying for a wide range of permeabilities with all other parameters held constant. Time required to dry a board to an average moisture content equal to FSP was compared to that criterion for a board with a saturated permeability of 10^{-12} cm^2; the result is shown in Fig. 10. It can be seen that at both very low and very high permeabilities, drying time asymptotically approaches a constant value. At low permeabilities, less than 10^{-14} cm^2; capillary-driven liquid transport is negligible and mass transport is due to diffusion; drying rate is controlled by diffusion rate. At high permeabilities, greater than 10^{-12} cm^2, the capillary transport is so large that moisture content is essentially uniform so that the drying rate is controlled at the surface by the convective mass transfer coefficient. At intermediate permeabilities, the drying rate is neither totally internally nor externally controlled, but is strongly dependent upon permeability. Since permeabilities measured for different wood species span this entire transition range [12], it cannot be overemphasized that good permeability data must be available before reasonable model results can be expected. This requirement is moderated somewhat in prediction of

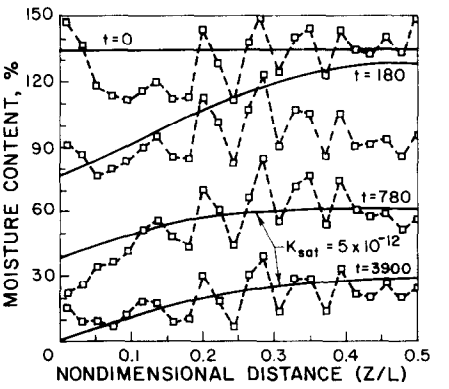

FIG. 9. Comparison of experimental and predicted moisture profiles for wood sample No. 113.

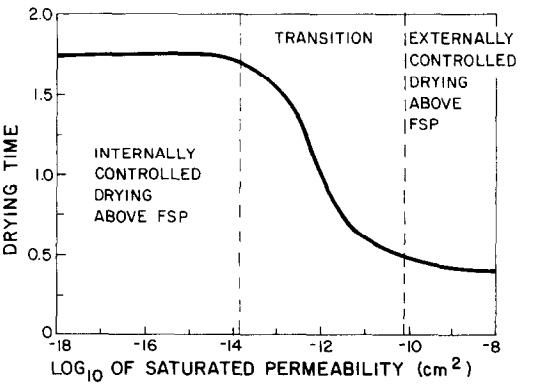

FIG. 10. The effect of permeability on drying time.

overall drying time (to well below FSP) because the diffusion-controlled late stage of drying always consumes a significant amount of the total drying time.

CONCLUSIONS

This work presents a model of the heat and mass transfer which occurs in wood during drying. Both diffusion and capillary transport mechanisms are included. A mechanistic model is utilized to relate the capillary porous properties of wood to known geometric and permeability parameters. Results generated from the model, when compared with experimental data, demonstrate that the model predicts reasonably well the drying rates and moisture distributions, provided accurate permeability data is available. If permeability values are in error, or if capillary transport is neglected altogether, then drying rates predicted by the model will be unrepresentative.

The model currently relies on an empirical function to predict the surface mass convection as a function of surface moisture content. This approach is severely limited in terms of general applicability without a definitive theory for mass transfer coefficients on partially wetted porous surfaces.

Acknowledgements—This material is based upon work supported in part by the National Science Foundation under Grant CME-7906361-01. Reviewers' comments which resulted in a revised and improved manuscript were greatly appreciated.

REFERENCES

1. T. K. Sherwood, The drying of solids—I, *Ind. Engng Chem.* **21,** 976–980 (1929).
2. C. A. Hart, The drying of wood, Technical Report No. 27, School of Forestry, North Carolina State University (1965).
3. A. V. Luikov, *Heat and Mass Transfer in Capillary-Porous Bodies.* Pergamon Press, Oxford (1966).
4. S. Whitaker, Simultaneous heat, mass, and momentum transfer in porous media: a theory of drying, *Adv. Heat Transfer* **13,** 119–203 (1977).
5. C. Skaar, *Water in Wood.* Syracuse University Press, New York (1972).
6. G. A Spolek, A model of convective, diffusive, and capillary heat and mass transport in drying wood. Ph.D. thesis, Washington State University (1981).
7. S. Whitaker, Heat and mass transfer in granular porous media. In *Advances in Drying* (edited by A. S. Mujumdar), Vol. 1. Hemisphere, Washington (1978).
8. R. E. Collins, *Flow of Fluids Through Porous Materials.* Reinhold, New York (1961).
9. S. Whitaker, Advances in theory of fluid motion in porous media, *Ind. Engng Chem.* **61,** 14–28 (1969).
10. J. F. Siau, *Flow in Wood.* Syracuse University Press, New York (1971).
11. J. Bear, *Dynamics of Fluids in Porous Media.* American Elsevier, New York (1972).
12. G. L. Comstock, Directional permeability of softwoods, *Wood Fiber* **1,** 283–289 (1970).
13. R. R. Stevens, Moisture above the fiber saturation point in loblolly pine sapwood. Ph.D. thesis, State University of New York (1972).
14. B. A. Olmstead, A model of heat and mass transfer in radially drying wood, TEL Report 82-14, Washington State University (1982).
15. G. A. Spolek and O. A. Plumb, Capillary pressure in softwoods, *Wood Sci. Technol.* **15,** 189–199 (1981).
16. A. J. Stamm, Permeability of wood to fluids, *Forest Prod. Jl* **13,** 503–507 (1963).
17. H. Resch and B. A. Ecklund, Permeability of wood—exemplified by measurements on redwood, *Forest Prod Jl* **14,** 199–206 (1964).
18. R. W. Meyer, Influence of pit aspiration on earlywood permeability of douglas fir, *Wood Fiber* **2,** 328–339 (1971).
19. G. A Spolek and O. A. Plumb, A numerical model of heat and mass transport in wood during drying. In *Drying '80* (edited by A. S. Mujumdar), Vol. 2, pp. 84–92 (1980).
20. O. A. Plumb and G. A. Spolek, An experimental study of convective heat and mass transfer coefficients during wood drying, TEL Report 80-12, Washington State University (1980).
21. C. A. Brown, Design and development of an experimental system employing gamma ray attenuation to investigate wood drying, TEL Report 81-20, Washington State University (1981).
22. O. A. Plumb, C. A. Brown and B. A. Olmstead, Experimental measurements of heat and mass transfer during convective drying of southern pine, *Wood Sci. Technol.* **18,** 187–204 (1984).
23. A. J. Stamm, Combined bound-water and water-vapor diffusion in Sitka Spruce, *Forest Prod. Jl* **10,** 644–648 (1960).
24. A. J. Stamm, *Wood and Cellulose Science.* Ronald Press, New York (1964).
25. C. A. Hart, Theoretical effect of gross anatomy upon conductivity of wood, *Forest Prod. Jl* **14,** 25–32 (1964).
26. H. P. Steinhagen, Thermal conductive properties of wood, green or dry, from −40 to 100°C: a literature review, USDA Forest Service General Technical Report, FDL-9 (1977).
27. R. H. Fleming and R. Revelle, Physical processes in the ocean, *Symposium on recent marine sediments* (edited by P. D. Trask), pp. 48–141. American Association of Petroleum Geologists (1939).

TRANSFERT DE CHALEUR ET DE MASSE PENDANT LE SECHAGE DU BOIS

Résumé—On développe un modèle de transfert de chaleur et de masse dans le traitement du bois. Il inclut le transport de liquide par action capillaire et par diffusion. Le modèle est unique dans le fait que les propriétés de transport qui ne sont parfois pas disponibles dans la littérature ou difficiles à mesurer, sont calculées à partir de la connaissance de la structure du bois. Des résultats calculés s'accordent avec ceux déterminés expérimentalement. Les résultats expérimentaux sont les premiers de leur genre par le fait que les profils d'humidité sont mesurés pendant le processus de séchage par atténuation gamma.

WÄRME- UND STOFFÜBERTRAGUNG BEI DER TROCKNUNG VON HOLZ

Zusammenfassung—Es wird ein Modell für den Wärme- und Stofftransport in Weichholz entwickelt. Das Modell berücksichtigt den Stofftransport durch Kapillarwirkung wie auch durch Diffusion. Das Modell ist einzigartig darin, daß die Transporteigenschaften, die in einigen Fällen sowohl nicht in der Literatur verfügbar wie auch schwierig zu messen sind, aus der Kenntnis der Holzstruktur berechnet werden. Die Rechenergebnisse stimmen vorzüglich mit den experimentell bestimmten überein. Die experimentellen Ergebnisse repräsentieren die ersten ihrer Art darin, daß die Feuchtigkeitsprofile während des Trocknungsprozesses mit Hilfe eines Gammastrahlenabsorptions-Verfahrens gemessen werden.

ТЕПЛО- И МАССОПЕРЕНОС ПРИ СУШКЕ ДРЕВЕСИНЫ

Аннотация—Разработана модель тепло-и массопереноса для мягкой древесины. Модель включает как капиллярный, так и диффузионный перенос жидкости. Она отличается тем, что трудные для измерения свойства переноса, которые в некоторых случаях отсутствуют в литературе, получены из данных о структуре древесины. Результаты расчетов хорошо согласуются с экспериментами. Экспериментальные данные являются первыми в своем роде, т.к. профили влажности измеряются в процессе сушки, исходя из затухания гамма излучения.